Living material assembly of bacteriogenic protocells

Can Xu

Centre for Protolife Research and Centre for Organized Matter Chemistry, School of Chemistry, University of Bristol, Bristol BS8 1TS, UK

Nicolas Martin

Univ. Bordeaux, CNRS, Centre de Recherche Paul Pascal, UMR5031, 115 Avenue du Dr Albert Schweitzer, 33600 Pessac, France

Mei Li

Centre for Protolife Research and Centre for Organized Matter Chemistry, School of Chemistry, University of Bristol, Bristol BS8 1TS, UK; School of Materials Science and Engineering, Shanghai Jiao Tong University, Shanghai, 200240, P. R. China

Stephen Mann (s.mann@bristol.ac.uk)

Centre for Protolife Research and Centre for Organized Matter Chemistry, School of Chemistry, University of Bristol, Bristol BS8 1TS, UK; School of Materials Science and Engineering, Shanghai Jiao Tong University, Shanghai, 200240, P. R. China; Max Planck-Bristol Centre for Minimal Biology, School of Chemistry, University of Bristol, Bristol BS8 1TS, United Kingdom https://orcid.org/0000-0003-3012-8964

Biological Sciences - Article

Keywords: protoliving micro-devices, artificial cells, bacteriogenic protocells

Posted Date: November 10th, 2021

DOI: https://doi.org/10.21203/rs.3.rs-959347/v1

Version of Record: A version of this preprint was published at Nature on September 14th, 2022. See the published version at https://doi.org/10.1038/s41586-022-05223-w.

Abstract

Advancing the spontaneous bottom-up construction of artificial cells with high organisational complexity and diverse functionality remains an unresolved issue at the interface between living and non-living matter. To address this challenge, a living material assembly process based on the capture and on-site processing of spatially segregated bacterial colonies within individual coacervate micro-droplets is developed for the endogenous construction of membrane-bounded, molecularly crowded, compositionally, structurally and morphologically complex synthetic cells. The bacteriogenic protocells inherit diverse biological components, exhibit multi-functional cytomimetic properties and can be endogenously remodelled to include a spatially partitioned DNA/histone nucleus-like condensate, membranized water vacuoles and a self-supporting 3D network of F-actin proto-cytoskeletal filaments. The ensemble is biochemically energized by self-sustainable ATP production derived from implanted live E. coli cells to produce a cellular bionic system with amoeba-like external morphology and integrated life-like properties. Our results demonstrate a novel bacteriogenic strategy for the bottom-up construction of functional protoliving micro-devices and provide opportunities for the fabrication of new synthetic cell modules and augmented living/synthetic cell constructs with potential applications in engineered synthetic biology and biotechnology.

Introduction

Establishing true-to-life functionality in synthetic cells is a global grand challenge that traverses multiple fields including synthetic biology, bioengineering and origins of life research.[1-5] The transitioning from inert capsule-based technologies to dynamical micro-compartmentalized entities capable of autonomous cytomimetic behaviour requires breakthrough advances in functional integration and on-board energization of multiplexed micro-systems. To date, the engineering of synthetic cellular systems (protocells) has been mainly approached using self-assembled vesicles,[6-8] semi-permeable microcapsules[9-15] and membrane-less or coated coacervate micro-droplets.[16-19] These compartments provide a controllable medium for the encapsulation and exchange of biological and non-biological components that are experimentally selected to demonstrate single functions such as gene expression,[6,9,20,21] enzyme catalysis[22] and ribozyme activity[23,24] within the synthetic cell models. Achieving high organisational and functional complexity in these constructs is methodological demanding due to difficulties in establishing sufficient compositional diversity and chemical complementarity by conventional methods of micro-compartmentalization under close-to-equilibrium conditions. These limitations restrict the structural and chemical complexity of current protocell models, inhibit the implementation of integrated componentry, and impede the development of energized cytomimetic systems.

To address these issues, herein we develop a radically new approach to engineer the first generation of energized protocells based on prokaryotes as structural and functional building blocks. In brief, we implement a living material assembly process for the bottom-up endogenous construction of

membrane-bounded molecularly crowded synthetic cells with multi-functional cytomimetic properties. Our approach is based on the co-capture and on-site processing of two spatially segregated bacterial colonies (*Escherichia coli* (*E. coli*) and *Pseudomonas aeruginosa* (*P. aeruginosa*, PAO1 strain) that are co-associated with individual poly(diallyldimethylammonium chloride) (PDDA)/adenosine 5'-triphosphate (ATP) coacervate micro-droplets. *In situ* lysis of the captured bacteria spontaneously gives rise to lipid membrane-coated protocells enclosing an extensive repertoire of functional biological components. We demonstrate that the bacteriogenic protocells are capable of complex processing such as the endogenous production of ATP via proto-metabolic activity (glycolysis) and inherit a sufficient complement of the bacterial gene expression machinery to implement *in vitro* transcription and translation. To increase the level of internal structural organization, we use a combination of endogenous polynucleotide liquid-liquid phase separation, ATP-driven supramolecular protein assembly and hypotonicity to augment the synthetic cells with a spatially partitioned nucleus-like DNA/histone condensate, 3D network of F-actin proto-cytoskeletal filaments and osmotically responsive membrane-bounded water vacuoles, respectively. As a step towards self-sustainable energization, we construct living/synthetic hybrids in which we exploit implanted live *E. coli* cells as surrogate mitochondria to increase and extend the endogenous production of ATP for enhancing kinase activity, glycolysis, *in vitro* gene expression and cytoskeletal assembly within the bacteriogenic protocells. The protoliving constructs adopt an amoeba-like external morphology and decreased membrane permeability due to on-site bacterial metabolism and growth to produce a cellular bionic system with integrated life-like properties. Taken together, our results demonstrate a novel bacteriogenic strategy for the bottom-up construction of functional protocellular micro-devices and provide opportunities for the fabrication of new synthetic cell modules and augmented living/synthetic cell constructs with potential applications in engineered synthetic biology and biotechnology.

Results

Assembly and construction of bacteriogenic protocells

To implement the endogenous assembly of bacteriogenic protocells, we first constructed a microscale building site comprising 5-30 μm-diameter pre-former coacervate droplets of spatially segregated live bacterial cells (**Fig. 1a**). Single populations of *E. coli* cells were sequestered at high concentrations into the interior of the membrane-free coacervate droplets within a few minutes to produce viable micro-compartmentalized colonies (**Fig**. **1b** and **Movie S1**). In contrast, PAO1 cells were almost instantaneously adsorbed onto the droplet surface to produce a shell of living bacteria (**Fig**. **1c** and **Movie S2**). Importantly, addition of a mixture of *E. coli* and PAO1 cells gave rise within a few minutes to single coacervate droplets comprising an internally segregated *E. coli* population surrounded by a thin continuous shell of PAO1 cells (**Fig 1d** and **Movie S3**). Quantitative FACS analysis of mixed suspensions of coacervate droplets and *E. coli* or PAO1 cells confirmed that the bacteria were captured at relatively high efficiency (typically 40-50%) after 5 min of incubation (**Figs 1e,f**). Similar experiments on droplets containing captured *E. coli* and PAO1 cells with expressed eGFP or mCherry fluorescence, respectively, indicated that the co-loading efficiency was *ca.* 15 % (**Fig**. **1g**). Corresponding time-dependent

fluorescence measurements on single coacervate droplets showed logistic growth rates in eGFP and mCherry fluorescence intensities up to threshold values as the droplet interior became filled with bacteria and assembly of the bacterial shell was completed (**Fig. 1h**). Staining the captured bacteria indicated that the majority of the cells associated with the coacervate droplets were alive (**Fig. S1**).

Having assembled the living pre-former droplets, we employed on-site processing to reconfigure and re-purpose the spatially segregated bacterial colonies into membrane-bounded, molecularly crowded protocells with complex microstructures and diverse bio-derived functionalities (**Fig. 2a**). To achieve this, we implemented the stepwise *in situ* lysis of the co-captured bacteria populations using a cell wall hydrolase (lysozyme) and antimicrobial peptide (melittin)[25] to release an extensive suite of bacterial membrane lipids/proteins and cytoplasmic components into the adjacent coacervate milieu (**Figs. S2, S3** and **S4**). While short lysis times generated coacervate droplets containing a living *E. coli* colony bounded by a 300-500 nm-thick shell of PAO1-derived membrane constituents, extending the processing time so that lysis of both types of bacteria occurred gave rise to structurally and compositionally complex protocells that consisted of a spatially segregated membrane of PAO1 lipids, which enclosed a coacervate matrix consisting principally of incarcerated *E. coli* cytoplasmic components along with PA01-membranized water vacuoles (**Figs. 2b-e** and **Figs. S5-S7**). Although proteins and polynucleotides did not readily leach from the protocells due to their strong affinity with the coacervate matrix (**Figs. 2c,d**), the PAO1-derived membrane was permeable to small molecule fluorescent dyes as well as macromolecular solutes, which could be readily taken up from the external solution (**Fig. S8**). The high membrane permeability was consistent with scanning electron microscopy images of freeze-dried bacteriogenic protocells, which showed a disordered arrangement of cytomembrane fragments on the surface of the droplets (**Fig. S9**). FACS quantitative analysis of samples prepared from co-captured *E. coli* and PAO1 cells with expressed eGFP and mCherry fluorescence, respectively, indicated that the percentage of bacteriogenic protocells produced after lysis was *ca*. 30% (**Fig. S10**)

Quantitative component analyses indicated that the bacteriogenic synthetic cells inherited protein, lipid, RNA and DNA contents of 16, 3, 3 and 1 wt%, respectively (**Fig. 2f**). Full protein typing was achieved by LC-MS proteomics, which indicated that approximately 78% (1359 proteins) of the combined library of bacterial proteins were retained by the protocells (**Fig. 2g**). Most (77%) of the retained proteins from the two populations were derived from the *E.coli* cells initially housed within the interior of the droplets. Of these, 92% of the *E. coli* protein types were associated with the protocells compared with only 49% of those in the PA01 proteome (**Fig. 2g**). In terms of molecular function, proteins with catalytic (43%), binding (32%) and structural (14%) roles were highly represented, whilst anatomical (48%) and intracellular entities (40%) along with protein-containing complexes (12%) were dominant as cellular components. These proteins were primarily associated with cellular (44%) and metabolic processes (40%), with the remaining proteins assigned principally to biological regulation, localization and sensing (**Fig. 2h**).

Bacteriogenic protocells as cytomimetic constructs

Given the extensive repertoire of biological components embodied within the bacteriogenic protocells, we sought to exploit the compositional complexity for the fabrication of synthetic cell modules with diverse cytomimetic properties operating at the level of individual enzymes, proto-metabolic pathways (glycolysis) and information networks (*in vitro* gene expression).

Retention of functional enzymes within the ensemble of released components was demonstrated by monitoring the activity of alkaline phosphatase, protease, lipase and β-galactosidase (β-gal) within the bacteriogenic protocells after exposure to appropriate fluorogenic small-molecule substrates in the external environment. In each case, production of the fluorescent outputs occurred homogeneously throughout the interior of the bacterially derived protocells and the products retained predominantly within the coacervate matrix (**Figs 3a-f**, **Movie S4** and **Figs. S11-13**). We also tested whether the bacteriogenic protocells inherited a sufficient complement of coordinated enzymes to implement the ten-enzyme cascade required for glycolysis.[26] For this, we added glucose-containing Luria-Bertani broth to protocells containing lactate dehydrogenase and assayed the onset of proto-metabolic activity via conversion of pyruvate to *L*-lactate along with formation of the reduced purple dye (formazan). Time-dependent spectroscopic measurements showed significant glycolysis activity in the protocell population (**Fig. 3g,h**), along with a blue-purple colouration and formation of insoluble formazan within their protocell interior (**Fig. 3i,j** and **Fig. S14**), indicating that sufficient levels of bacterially derived cell respiration components were released by lysis and retained within the cytoplasmic-like coacervate matrix.

As bacterial lysates can be used for *in vitro* translation/transcription,[27] we loaded selected components of an expression system (buffer, T7 promoters and polymerases, amino acids, nucleotides and t-RNA) and a plasmid (pEXP5-NT/deGFP) for deGFP expression into PDDA/ATP coacervate droplets. Notably, the bacterial lysate accompanying the cell-free expression kit was not included. We then used the primed droplets to capture *E. coli* and PAO1 cells followed by *in situ* lysis, bacteriogenic protocell construction and storage on ice. As a consequence, subsequent endogenous processing of the incorporated plasmid by the protocells was dependent on inheriting a sufficient complement of gene expression machinery (peptidyl transferase, RNA synthetases, energy generation, translation factors (IF1, IF2, IF3), ribosomal proteins etc) from *in situ* lysis of the bacterial cells. Gene expression was initiated by raising the temperature to 37 °C with additional feed buffer added after 30 min to sustain the system. Production of deGFP occurred specifically within the bacteriogenic protocells over 5 hours to give a protein yield of 0.01 μM with maximum and minimum expression rates at 0.5 and 3 h, respectively (**Fig. 3k-m**). In contrast, negligible green fluorescence was observed for synthetic cells lacking the pEXP5-NT/deGFP plasmid (**Fig. 3m**). Gel electrophoresis of the extracted proteins showed a band at 35 kDa that was absent without the plasmid (**Fig. 3n**), and Western blotting images indicated that the 35 kDa band was stained on exposure to an anti-GFP antibody (**Fig. 3o**), confirming deGFP expression within the bacteriogenic protocells.

On-site augmentation of bacteriogenic protocells

Bacterially derived synthetic cells containing both a spatially partitioned nucleus-like organelle and 3D structural network of proto-cytoskeletal filaments were prepared by endogenous remodelling of the cytoplasmic-like interior (**Fig. 4a**). Spontaneous aqueous two-phase liquid-liquid separation of a single bacterial DNA/histone condensate within the bacteriogenic protocells was achieved within the cytoplasmic-like interior by uptake of carboxymethyldextran (CM-dextran; 70 kDa). The procedure, which was dependent on the presence of linear double-stranded (*ds*) DNA and initially developed using native PDDA/ATP droplets (**Figs. S15-17**), involved loading the coacervate droplets with a histone protein (type II-A) and a mixture of DNAase I and $MnCl_2$ – the latter used to cleave the native bacterial plasmid DNA into linear fragments. This was followed by capture of a mixed population of *E. coli*/PA01 cells and release of the bacterial plasmid DNA (and other cytoplasmic components) by lysis to generate a homogeneous distribution of a linear DNA/histone complex within the protocell interior. Subsequent addition of CM-dextran and diffusion of the polysaccharide through the outer PA01-derived membrane resulted in the nucleation of a single membrane-free DNA/histone condensate inside the individual protocells within a few tens of seconds (**Figs. 4b,c**). Essentially all the released bacterial DNA (99%) was confined to the nucleus-like condensate while most (75%) of the released bacterial proteins were sequestered into the molecularly crowded cytoplasmic-like region of the protocells (**Figs. 4d,e**). Similar experiments involving bacterially derived protocells without pre-loaded DNAase I and $MnCl_2$ resulted in the nucleation of large numbers of small (0.3-2 μm) plasmid DNA/histone condensates throughout the CM-dextran-enriched phase (**Fig. 4e** and **Fig. S18**). When exposed to hypotonic conditions, the remodelled protocells were further elaborated with membrane-coated water vacuoles to produce synthetic cells that exhibited multiple types of spatially segregated cytomimetic structures (**Figs 4f,g**).

Having established a protocol for the *in situ* condensation and spatial localization of bacterial DNA within the protocells, we sought to re-structure the molecularly crowded proto-cytoplasmic region by on-site energy-driven supramolecular assembly of a F-actin cytoskeletal-like filamentous network to produce self-supported cytomimetic models. Initial experiments using PDDA/ATP pre-former coacervate droplets indicated that G-actin and Mg^{2+} ions were readily taken up by the bacteriogenic protocells and that *in situ* F-actin assembly was activated endogenously by the coacervate-derived ATP (**Fig. S19**). However, as only short filaments of F-actin were produced due to the high native ATP concentration (*ca*. 200 mM),[28] we prepared the sub-compartmentalized bacteriogenic protocells using PDDA/uridine-5'-triphosphate (UTP) coacervate droplets (**Fig. S20**) and pre-loaded the droplets with an enzyme-based ATP-generating system based on pyruvate kinase (PK), phosphoenolpyruvate (PEP) and ADP (**Fig. 4i**).[29] Subsequent uptake of G-actin and Mg^{2+} initiated F-actin assembly specifically within the synthetic cells and transformed the bacteriogenic constructs into hydrogelled microstructures with retention of the spherical morphology (**Fig. 4j**). The results indicated that the on-board generation of ATP arising from the encapsulated PK/PEP/ADP cascade over a period of approximately 20 min was sufficient to produce the controlled restructuring of the protocell interior. This was confirmed by confocal fluorescence microscopy images of single protocells, which showed the presence of a localized low-density network of F-actin micro-filaments specifically dispersed within the proto-cytoplasmic region but not in the phase-separated DNA/histone sub-compartment (**Figs. 4k-m** and **Fig. S21**).

Live cell energization and reconfiguration of bacteriogenic protocells

Given the potential for compositional, structural and functional complexity in the bacteriogenic protocells, we sought to couple these attributes to an internal ATP-based energy source as a step to increasing the autonomy and self-sufficiency of the life-like constructs. To achieve this, we implanted *E. coli* cells into PDDA/UTP-based bacteriogenic protocells (**Fig. 5a**), and used the incarcerated living cells as surrogate mitochondria for the endogenous production of ATP. Confocal fluorescence microscopy images indicated that the *E. coli* cells were sequestered specifically into the cytoplasmic-like space; in contrast, no cells were observed in the DNA/histone-enriched proto-nucleus (**Fig. 5b**). Typically, 10-50 bacteria were initially captured within the cellular bionic system. Live/dead staining of the constructs indicated that many of the implanted *E. coli* cells remained viable after entrapment for 3 h (**Fig. S22**). Corresponding time-dependent FACS data indicated that the population of *E. coli* cells increased approximately 10 times over a period of 48 h with the percentage of live cells decreasing from 99 (1 h) to 60 % (48 h) (**Fig. 5c and d and Fig. S23**). Growth of the trapped bacterial colony produced a three-fold increase in the total protein concentration within the protocells over a period of 48 h (**Fig. 5e**).

To energize the living/synthetic cell construct, we initiated ATP production in the incarcerated *E. coli* cells by addition of glucose (in Luria-Bertani broth) and exploited the extracellular secretion of the energy-rich mononucleotide[30] to chemically charge the co-located bacteriogenic protocells (**Fig. S24**). Consequently, continuous biologically mediated ATP production in the PDDA/UTP-based bacteriogenic protocells was sustained for up to 36 h compared with 20 minutes in the presence of a sequestered PK/PEP/ADP enzyme-based pathway (**Fig. 5f**). Bioproduction of ATP was fitted to an exponential decay curve that attained equilibrium after *ca*. 36 h with a maximum ATP concentration of 1.65 mM under the conditions typically employed (**Fig. S25**). Importantly, ATP bio-generation within the hybrid protocells was readily sustained by replenishing the nutrients in the external medium, whilst addition of new substrates (ADP, PEP) to the enzyme-based pathway disrupted the structural integrity of the protocells.

Bio-generation and extracellular secretion of ATP resulted in prolonged enzyme activity and gene expression, as well as increased levels of F-actin polymerization in the living/synthetic constructs. For example, kinase activity was approximately doubled when compared to PDDA/UTP bacteriogenic protocells containing released bacterial lysate (no live *E. coli* cells) and increased 1.3-fold in comparison with the implanted PK/PEP/ADP pathway (no live *E. coli* cells) (**Fig. 5g** and **Fig. S26**). *In vitro* gene expression of deGFP was extended from 3 to 24 h with a final deGFP concentration of *ca*. 0.015 μM (**Fig. 5h,l** and **Fig. S27**) and pyruvate production was increased 1.7-fold due to sustained glycolysis in the implanted bacteria (**Fig. S28**). On-site assembly of F-actin after passive uptake of G-actin and Mg^{2+} ions gave rise to an extensive network of protein filaments that filled most of the proto-cytoplasmic space within 30 min (**Figs. 5j,k** and **Fig. S29**). Compared with supramolecular polymerization driven by the loaded PK/PEP/ADP cascade, living cell ATP production gave rise to a considerably higher density matrix of F-actin filaments that unlike the enzyme-supplemented pathway filled the proto-cytoplasmic space after 0.5 h (**Fig. S30**). As a consequence, living bacteria, a single DNA/histone sub-compartment and

water vacuoles were immobilized in the cytoskeletal-like framework to produce a self-supporting cellular bionic systems that remained structurally intact in water and salt solutions for at least 7 days (**Fig. 5l** and **Fig. S31**). In contrast, living/synthetic constructs prepared without F-actin were only stable for up to 3 days in buffer and disassembled immediately under hypertonic conditions (**Fig. S31**).

Finally, we sought to exploit the continuous bio-generation of metabolic products within the bacteriogenic protocells to implement changes in membrane interfacial tension as a step towards producing living/synthetic cell hybrids with non-spherical morphology. In the absence of incarcerated *E. coli* cultures, mounting the F-actin containing spherical bacteriogenic protocells onto pegylated glass substrates and leaving the samples at room temperature in Luria-Bertani (LB) broth for 48 h resulted in minimal changes in structure and morphology (**Fig. S32**). In contrast, similar experiments with bacteriogenic protocells containing encapsulated live *E. coli* cells and a F-actin network gave rise to progressive changes in morphology (**Fig. 6a**). Within 48 h, most of the spherical microstructures adopted a more irregular cell-like form whilst maintaining their complex internal organization and outer membrane structure (**Fig. 6b**). During this period, the average number of *E. coli* cells per protocell increased approximately eight-fold within the first 24 h, after which the entrapped population of live cells decreased by approximately 35% after 48 h (**Fig. 6c**). Growth of the bacteria was associated with a two-fold increase in the average protocell volume over 48 h (**Fig. 6d**).

Given that the amoeba-like morphology was also observed after 24-48 h for living cell/protocell constructs prepared without a F-actin network (**Fig. S32**), we ruled out the possibility that the changes in form were associated with anisotropic mechanical forces induced by formation of the cytoskeletal-like matrix. In addition, no morphological changes were observed after short periods (1 h) when the bacteriogenic protocells were loaded with extremely high loadings of freshly washed *E.coli* cells (**Fig. S32**), suggesting that prolonged metabolic activity of the incarcerated bacterial cells, rather than an increase *per se* in the population density within the protocells, was responsible for the transition to the amoeba-like form. Although, time-dependent increases in bulk wettability were observed for single droplets of concentrated suspensions of the living/synthetic hybrids mounted on pegylated glass slides (**Fig. S33**), mounting the same constructs onto hydrophobic plastic or non-modified glass surfaces also showed amoeba-like morphologies after 48 h incubation, indicating that specific interactions with the substrate were not critical in determining the shape change (**Fig. S34**). Indeed, low resolution confocal microscopy images of the living/synthetic constructs recorded in aqueous suspension also showed the non-spherical morphology (**Fig. S35**), in agreement with an endogenous mechanism associated with prolonged activity of the entrapped *E. coli* cells. Interestingly, the permeability of the outer membrane to macromolecular diffusion decreased markedly with change of shape such that dextran above a molecular weight of 10 kDa, BSA-FITC (66 kDa) and single-stranded DNA (8 kDa) were no longer taken up into living/synthetic hybrids that were biologically active for more than 20h (**Figs. 6e-h** and **Fig. S36**). Based on these observations, we speculate that the continuous production of bacterial lipids facilitated partially sealing of defects in the outer membrane, as well as increasing membrane surface area and elasticity.

Discussion

An ensemble of cytomimetic features is integrated into a synthetic cell construction pathway by using a living material assembly process in which prokaryotes are employed as on-site repositories of key structural and functional building units. Depending on the extent of the construction process, a total of seven distinct cytomimetic attributes can be integrated into the bacteriogenic protocells (**Figs. 6i,j**). Implementation of the basic processing strategy gives rise to complex synthetic cells with a bacterially derived semi-permeable outer membrane and internal molecularly crowded proto-cytoplasm containing a PDDA/ATP (UTP) coacervate, an extensive suite of bacterial proteins and polynucleotides, a functional metabolic network and intact translation/transcription machinery. Further elaboration of the synthetic cells can be achieved endogenously by structural augmentation with a single membrane-free DNA/histone nucleus-like condensate; osmotically responsive membrane-bounded water vacuoles and a primitive F-actin cytoskeletal-like network; in each case, the additional design features are implemented without compromising the multiple cytomimetic functions. Higher-level operations are introduced by using implanted live *E. coli* cells as surrogate mitochondria for energization, which prolongs ATP bioproduction and transforms the spherical bacteriogenic protocells into a cellular bionic system with amoeba-like cell morphology.

A critical aspect of the living material construction sequence is the spontaneous coacervate droplet-mediated capture and spatial segregation of *E. coli* and PA01 cells that together enable on-site processing and retention of diverse bacterial components for synthetic cell elaboration. The methodology opens the possibility of high levels of programmability by using engineered bacteria designed to deliver specialized components and biological processes for establishing robust metabolic networks and genetic circuitry in the bacteriogenic protocells. Additionally, the spatial arrangement of live *E. coli* and PA01 cells in the initial pre-former coacervate droplets could be modulated by changes in the coacervate composition (**Fig. S37**), suggesting that the construction sequence could be adapted in the future to fabricate complex synthetic cells with alternative types of bacteriogenic organization.

Finally, we expect our new living material assembly approach to provide opportunities for the bottom-up construction of highly integrated synthetic cells and augmented living/synthetic cell constructs. For example, the possibility of spatially coupling F-actin polymerization to the membrane of the bacteriogenic protocells or embedded vacuoles could lead to life-like micro-devices with mechanically adaptive properties, while information processing derived from the DNA/histone proto-nuclei could be a first step to a rudimentary “proto-eukaryote” cell. From a cellular bionics perspective, the potential for symbiosis in living/synthetic cell hybrids constructed from bacterially derived construction pathways could offer more complex modules for development in diagnostic and therapeutic areas of synthetic biology as well as in biomanufacturing and biotechnology in general.

Declarations

Acknowledgements

We thank Dr Y. Takebayashi and Prof James Spencer, and Dr E. Bragginton, School of Cellular and Molecular Medicine, University of Bristol for help with bacterial cultures and Western blot analysis, respectively. We thanks Dr A. Coutable and Prof J. L. R. Anderson, School of Biochemistry, University of Bristol for providing plasmid pEXP5-NT/deGFP,

Author contributions

C.X., M.L. and S.M. conceived the experiments. C.X. and N.M. performed the experiments. C.X. and M.L. undertook the data analysis. C.X., M.L. and S.M. wrote the manuscript.

Competing interests

The authors declare no competing interests.

Additional information

Methods, including statements of data availability and any associated accession codes and references, are available in the online version of this paper.

References

1 Building a Synthetic Cell, https://www.basyc.nl; The Synthetic Cell Initiative, https://www.syntheticcell.eu/about-the-initiative/; Build-A-Cell, https://www.buildacell.org.

2 van Stevendaal, M. H. M. E., van Hest, J. C. M. & Mason, A. F. Functional Interactions Between Bottom-Up Synthetic Cells and Living Matter for Biomedical Applications. *ChemSystemsChem* **3,** e2100009, (2021).

3 Jeong, S., Nguyen, H. T., Kim, C. H., Ly, M. N. & Shin, K. Toward Artificial Cells: Novel Advances in Energy Conversion and Cellular Motility. *Advanced Functional Materials* **30**, 1907182, (2020).

4 Toparlak, O. D. & Mansy, S. S. Progress in synthesizing protocells. *Experimental Biology and Medicine* **244**, 304-313, (2018).

5 Yewdall, N. A., Mason, A. F. & van Hest, J. C. M. The hallmarks of living systems: towards creating artificial cells. *Interface Focus* **8**, 20180023, (2018).

6 Adamala, K. P., Martin-Alarcon, D. A., Guthrie-Honea, K. R. & Boyden, E. S. Engineering genetic circuit interactions within and between synthetic minimal cells. *Nature Chemistry* **9**, 431-439, (2017).

7 Deng, N.-N., Yelleswarapu, M., Zheng, L. & Huck, W. T. S. Microfluidic Assembly of Monodisperse Vesosomes as Artificial Cell Models. *Journal of the American Chemical Society* **139**, 587-590, (2017).

8 Weiss, M. *et al.* Sequential bottom-up assembly of mechanically stabilized synthetic cells by microfluidics. *Nature Materials* **17**, 89-96, (2018).

9 Huang, X. *et al.* Interfacial assembly of protein–polymer nano-conjugates into stimulus-responsive biomimetic protocells. *Nature Communications* **4**, 2239, (2013).

10 Li, M., Harbron, R. L., Weaver, J. V. M., Binks, B. P. & Mann, S. Electrostatically gated membrane permeability in inorganic protocells. *Nature Chemistry* **5**, 529-536, (2013).

11 Marguet, M., Bonduelle, C. & Lecommandoux, S. Multicompartmentalized polymeric systems: towards biomimetic cellular structure and function. *Chemical Society Reviews* **42**, 512-529, (2013).

12 Niederholtmeyer, H., Chaggan, C. & Devaraj, N. K. Communication and quorum sensing in non-living mimics of eukaryotic cells. *Nature Communications* **9**, 5027, (2018).

13 Kumar, B. V. V. S. P., Patil, A. J. & Mann, S. Enzyme-powered motility in buoyant organoclay/DNA protocells. *Nature Chemistry* **10**, 1154-1163, (2018).

14 Mukwaya, V. *et al.* Lectin-Glycan-Mediated Nanoparticle Docking as a Step toward Programmable Membrane Catalysis and Adhesion in Synthetic Protocells. *ACS Nano* **14**, 7899-7910, (2020).

15 Dou, H. *et al.* Higher-order assembly of crystalline cylindrical micelles into membrane-extendable colloidosomes. *Nature Communications* **8**, 426, (2017).

16 Martin, N. Dynamic Synthetic Cells Based on Liquid–Liquid Phase Separation. *ChemBioChem* **20**, 2553-2568, (2019).

17 Zhang, Y. *et al.* Giant Coacervate Vesicles As an Integrated Approach to Cytomimetic Modeling. *Journal of the American Chemical Society* **143**, 2866-2874, (2021).

18 Tang, T.-Y.D. *et al.* Fatty acid membrane assembly on coacervate microdroplets as a step towards a hybrid protocell model. *Nature Chemistry* **6**, 527-533, (2014).

19 Koga, S., Williams, D. S., Perriman, A. W. & Mann, S. Peptide–nucleotide microdroplets as a step towards a membrane-free protocell model. *Nature Chemistry* **3**, 720-724, (2011).

20 Tang, T.-Y.D., van Swaay, D., deMello, A., Ross Anderson, J. L. & Mann, S. In vitro gene expression within membrane-free coacervate protocells. *Chemical Communications* **51**, 11429-11432, (2015).

21 Li, M., Green, D. C., Anderson, J. L. R., Binks, B. P. & Mann, S. In vitro gene expression and enzyme catalysis in bio-inorganic protocells. *Chemical Science* **2**, 1739-1745, (2011).

22 Küchler, A., Yoshimoto, M., Luginbühl, S., Mavelli, F. & Walde, P. Enzymatic reactions in confined environments. *Nature Nanotechnology* **11**, 409-420, (2016).

23 Strulson, C. A., Molden, R. C., Keating, C. D. & Bevilacqua, P. C. RNA catalysis through compartmentalization. *Nature Chemistry* **4**, 941-946, (2012).

24 Drobot, B. *et al.* Compartmentalised RNA catalysis in membrane-free coacervate protocells. *Nature Communications* **9**, 3643, (2018).

25 Faust, J. E., Yang, P.-Y. & Huang, H. W. Action of Antimicrobial Peptides on Bacterial and Lipid Membranes: A Direct Comparison. *Biophysical Journal* **112**, 1663-1672, (2017).

26 Gray, L. R., Tompkins, S. C. & Taylor, E. B. Regulation of pyruvate metabolism and human disease. *Cellular and Molecular Life Sciences* **71**, 2577-2604, (2014).

27 Silverman, A. D., Karim, A. S. & Jewett, M. C. Cell-free gene expression: an expanded repertoire of applications. *Nature Reviews Genetics* **21**, 151-170, (2020).

28 Fung, B. M. & Eyob, E. The effect of ATP concentration on the rate of actin polymerization. *Archives of Biochemistry and Biophysics* **220**, 370-378, (1983).

29 Nakashima, K. K., Baaij, J. F. & Spruijt, E. Reversible generation of coacervate droplets in an enzymatic network. *Soft Matter* **14**, 361-367, (2018).

30 Alvarez, C. L. *et al.* Dynamic regulation of extracellular ATP in Escherichia coli. *Biochemical Journal* **474**, 1395-1416, (2017).

Figures

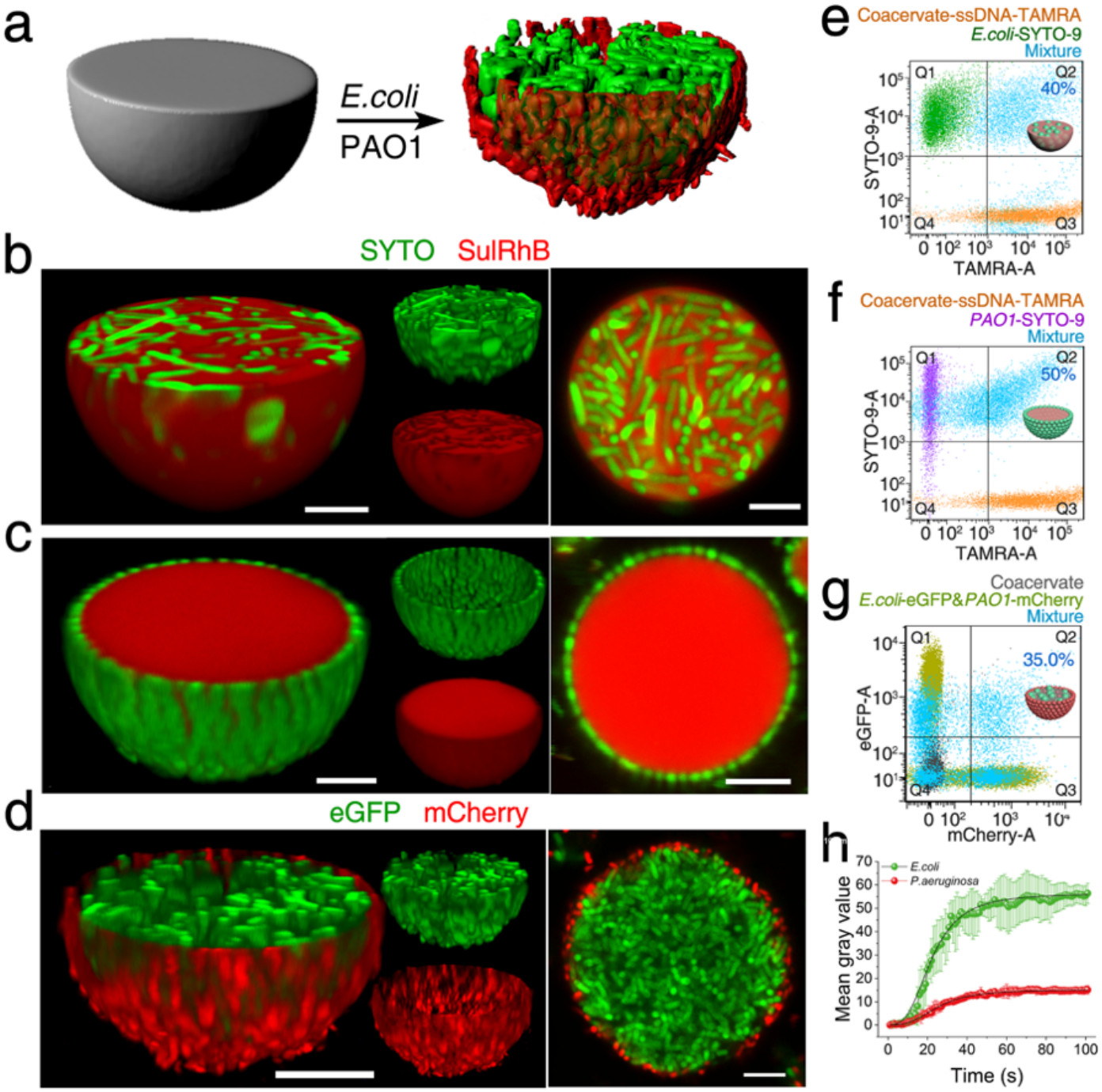

Figure 1

Spontaneous capture of bacterial colonies in coacervate micro-droplets. a, Graphic showing specific uptake or surface-adsorption of living E. coli (green) and PAO1 (red) cells, respectively, in PDDA/ATP coacervate micro-droplets. b-d, Confocal microscopy images of coacervate droplets after spontaneous capture of living E. coli (b), PAO1 (c), and a binary population of E. coli and PAO1 (d) cells. 3D (left) and 2D (right) fluorescence images; green/red fluorescence overlays, and filtered images are shown. Fluorescence labels in (b,c); coacervate (Sul-RhB, red fluorescence), bacteria (SYTO-9, green fluorescence, DNA stain). Green and red fluorescence in (d) originate from expressed eGFP and mCherry. Scale bars, 5 μm. e-g, FACS fluorescence gated analysis of ssDNA-TAMRA-doped coacervate micro-droplets (orange

dots, red fluorescence), SYTO 9-stained E.coli (green dots, green fluorescence) and labelled droplets with captured E.coli-SYTO (blue dots, red and green fluorescence) (e); ssDNA-TAMRA-droplets (orange dots), SYTO 9-stained PAO1 (purple dots) and labelled droplets with captured PAO1-SYTO 9 (blue dots) (f); non-fluorescent coacervate micro-droplets (grey dots), a binary population of E.coli-GFP and PAO1-mCherry cells (olive green dots, green and red fluorescence, no coacervate) and unlabelled droplets with co-captured populations of E.coli-GFP and PAO1-mCherry cells (blue dots, green and red fluorescence) (g). Free E.coli bacteria (46%, gate Q1), free droplets (12%, Q3), droplets with captured bacteria (40%, Q2) (e); 42 (PAO1), 7 and 50 % (f). Impurities (Q4), 2% in both cases. Free E. coli-eGFP (33%, gate Q1), free PAO1-mCherry (22%, Q3), free unlabelled droplets (10%, Q4), and droplets with co-captured bacteria (35%, Q2) (g). Data were recorded after 5 min for a total population size of 1 x 106. h. Time-dependent fluorescence plots of the co-capture of E. coli (green) and PAO1 (red) cells in individual coacervate droplets. Curves are fitted to logistic sigmoid functions; E. coli and PAO1 time midpoints (t1/2), 22 and 25 s; growth rate indices, 1.75 and 5.9; equilibrium times (first derivative ≈ 0) ca. 70 and 80 s, respectively. Number of protocells measured, n = 4; errors bars, standard deviations.

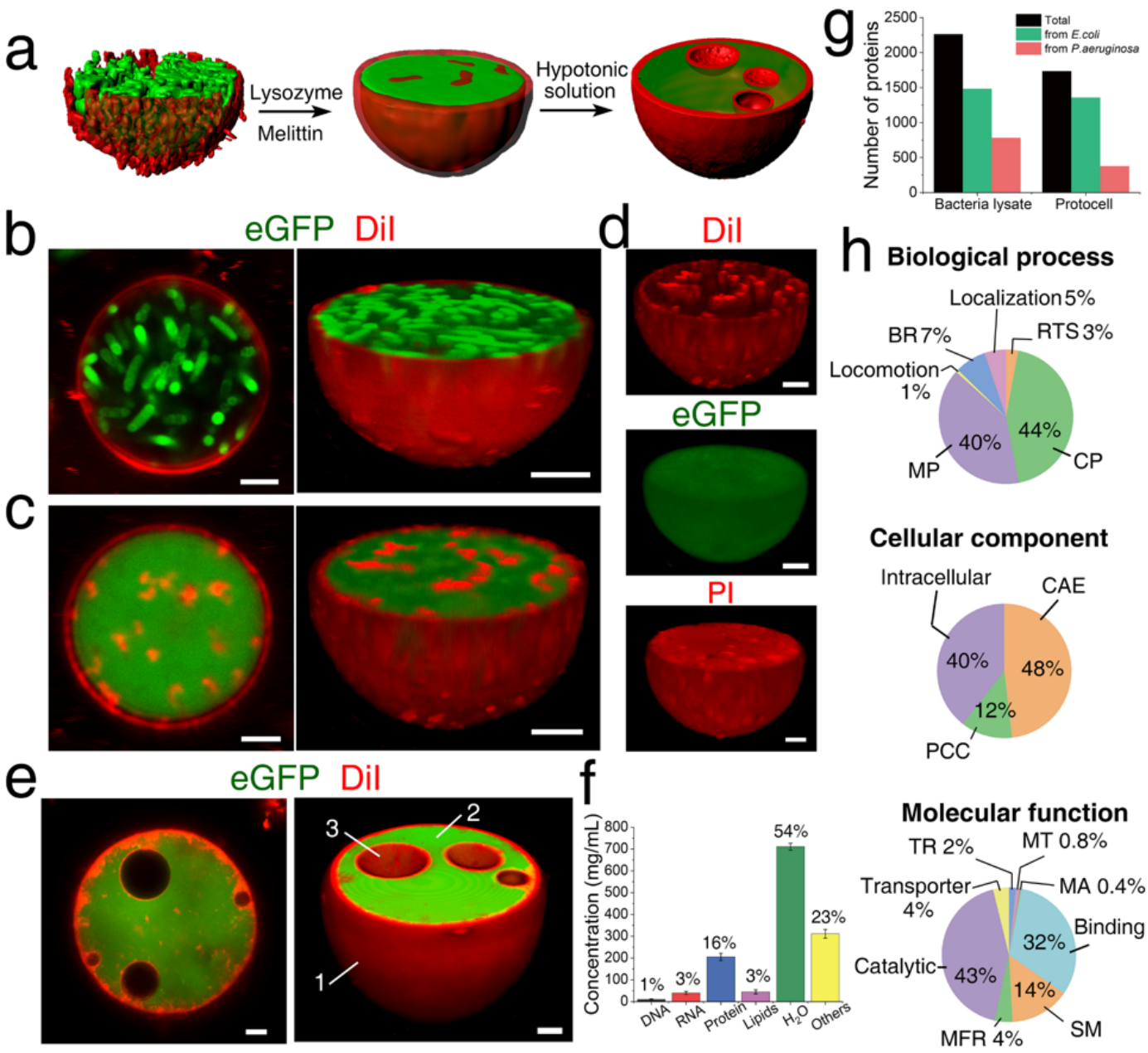

Figure 2

Construction of bacteriogenic protocells. a, Graphic showing on-site bio-processing of living pre-former coacervate droplets into bacteriogenic protocells comprising encapsulated E. coli-derived cytoplasmic components (green) surrounded by a continuous PA01-derived membrane (red) (left and middle). Exposure to hypertonic conditions results in water vacuole formation within the protocells (right). b-d, 2D and 3D green/red overlaid confocal fluorescence microscopy images of single PDDA/ATP coacervate droplets containing spatially separated populations of living E.coli-eGFP (green fluorescence) and lysed PAO1 cells (red fluorescence, DiI C18 stain, lipid fragments) (b), and after lysis of both bacteria to produce a bacteriogenic protocell (c,d). Some cytomembrane fragments are present within the protocell (d, upper image) along with homogeneous distributions of E. coli-derived eGFP (d, middle) and DNA (d, lower, PI-red fluorescence). e, 2D (left) and 3D (right)confocal fluorescence microscopy images of an individual

bacteriogenic protocell containing membrane-coated water-filled vacuoles (non-fluorescent region). Labels: 1, “proto-cytomembrane”; 2, “proto-cytoplasm”; 3, water-filled vacuole. Staining as in (c). Scale bars in b-f, 5 μm. f, Quantitative component analyses of bacteriogenic protocells derived from lysed mixed populations of E. coli and PAO1 cells. g, LC-MS proteomic analyses obtained for samples of bacteriogenic protocells and a binary population of E.coli and PAO1 cells (no coacervate droplets). Contaminating proteins/peptides such as lysozyme and melittin were excluded from the analysis. h. Gene Ontology (GO) term annotation and functional classification for identified proteins associated with bacteriogenic protocells. The proteins were identified in multiple sub-categories (biological processes (left), cellular components (middle) and molecular functions (right). Labels: BR, biological regulation; MP, metabolic process; RTS, response to stimulus; CP, cellular process., CAE, cellular anatomical entity; PCC, protein-containing complex; TR. translation regulator; MT, molecular transducer; MA, molecular adaptor; SM, structural molecule; MFR, molecular function regulator.

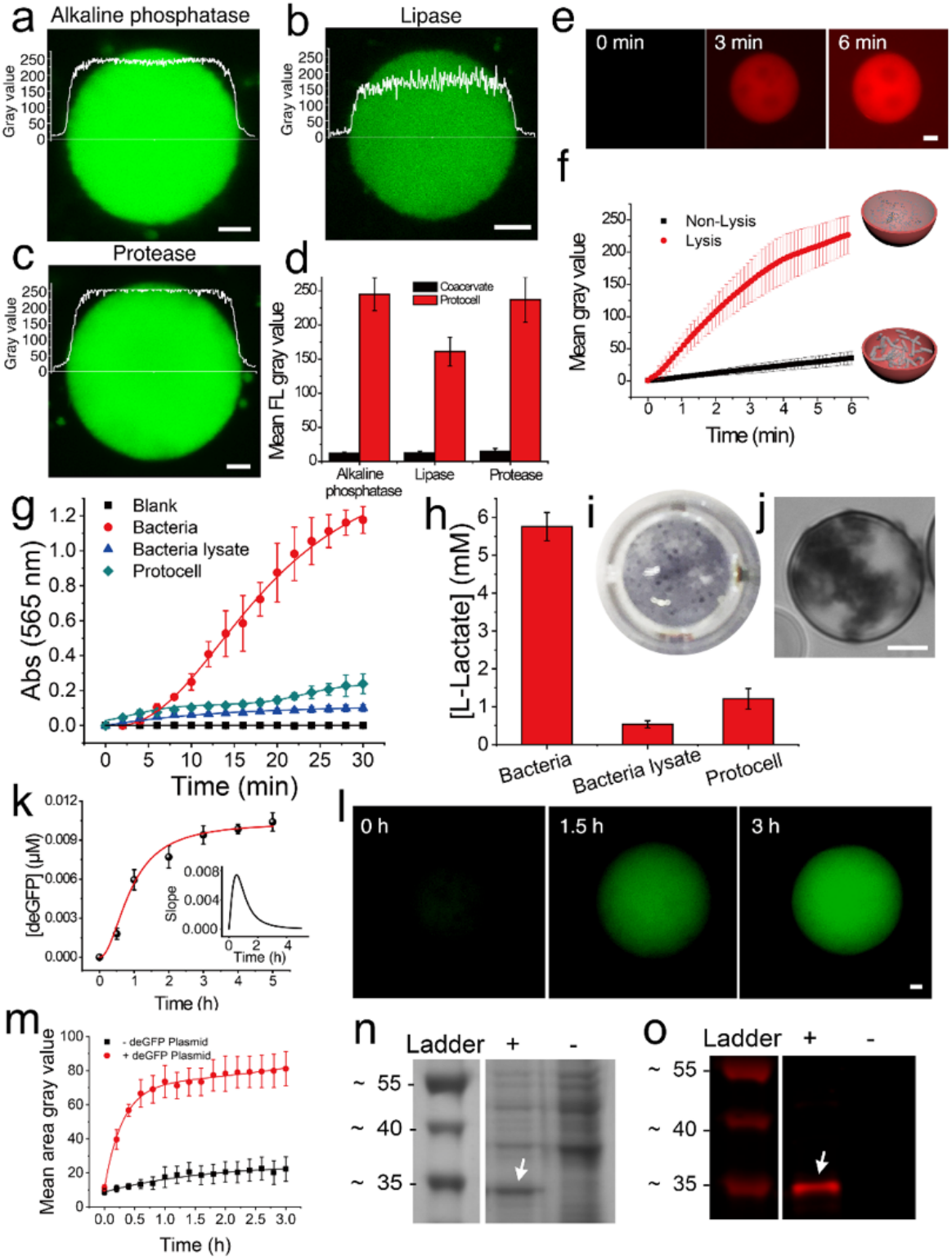

Figure 3

Cytomimetic properties of bacteriogenic protocells. a-c, Confocal fluorescence microscopy images of single protocells containing bacterially derived alkaline phosphatase (a), lipase (b) and protease (c) recorded 30 min after exposure to fluorescein diphosphate (non-fluorescent) (a), BODIPY® FL dye-labelled triacylglycerol-based EnzChek lipase substrate (quenched fluorescence) (b), and BODIPY® FL dye-labelled casein derivative (quenched fluorescence) (c), showing production and sequestration of

fluorescence products (fluorescein (a) and free BODIPY® FL dye (b and c) throughout the cytoplasmic-like interior. d, Corresponding mean grey values for reactions shown in (a-c) and for native coacervate droplet controls. e, Time-dependent fluorescence microscope images of a single bacteriogenic protocell after addition of resorufin-β-D-galactopyranoside (RBG), showing endogenous β-gal-mediated production of resorufin (red fluorescence). f, Plots of mean grey value with time recorded from fluorescence images of single bacteriogenic protocells (red) or single coacervate droplets with co-captured non-lysed bacteria (black) after addition of RBG showing β-gal activity only after lysis and construction of the protocells; n = 3. g, Time-dependent plots of changes in absorption at 565 nm (formazan production) for native coacervate droplets (black squares), bacterial lysate (no droplets, blue triangles), bacteriogenic protocells (grey diamonds), live E. coli and PAO1 cells (2 : 1; OD = 1, red circles) after addition of Luria-Bertani broth. Lysate and protocells were generated from the same bacterial concentrations as used in the cell samples. Number of experiments, n = 3. h, Final concentrations of L-lactate produced in experiments shown in g. Protocell glycolysis is ca. 80% lower than for the living cells and ca. 3-fold higher than the bacterial lysate due to preferential partitioning of enzymes, nutrients and substrates within the coacervate matrix after release from the bacterial cells. i, Photograph of a sample well containing a suspension of protocells after glycolysis. Larger protocells can be observed as purple dots (formazan) dispersed throughout the well. j, Confocal bright field image of a single bacteriogenic protocell 0.5 h after glycolysis showing formation of the assay product formazan within the cytoplasmic-like interior. k, Plot showing time-dependent increase in deGFP concentration for a population of bacteriogenic protocells undergoing endogenous in vitro gene expression. The data are fitted to a Hill function (t1/2 = 0.9 h, Hill coefficient = 2). Number of experiments, n= 2; error bars, standard deviations. l, Time-dependent fluorescence microscopy images of a single bacteriogenic protocell showing progressive increase in expressed deGFP (green fluorescence) throughout the cytoplasmic-like interior. n= 3; error bars, standard deviations. m, Plots of mean grey values with time recorded from green fluorescence (deGFP) images of single bacteriogenic protocells with (red) or without (black) plasmid pEXP5-NT/deGFP. n,o Gel electrophoresis profiles (n) and Western blotting images (o) of extracted proteins obtained after salt-induced disassembly of protocells with (+) or without (-) plasmid pEXP5-NT/deGFP. Arrows in (o) show additional band at 35 kDa that was observed only with the plasmid, and which stains on exposure to an anti-GFP antibody (right panel). All scale bars are 5 μm.

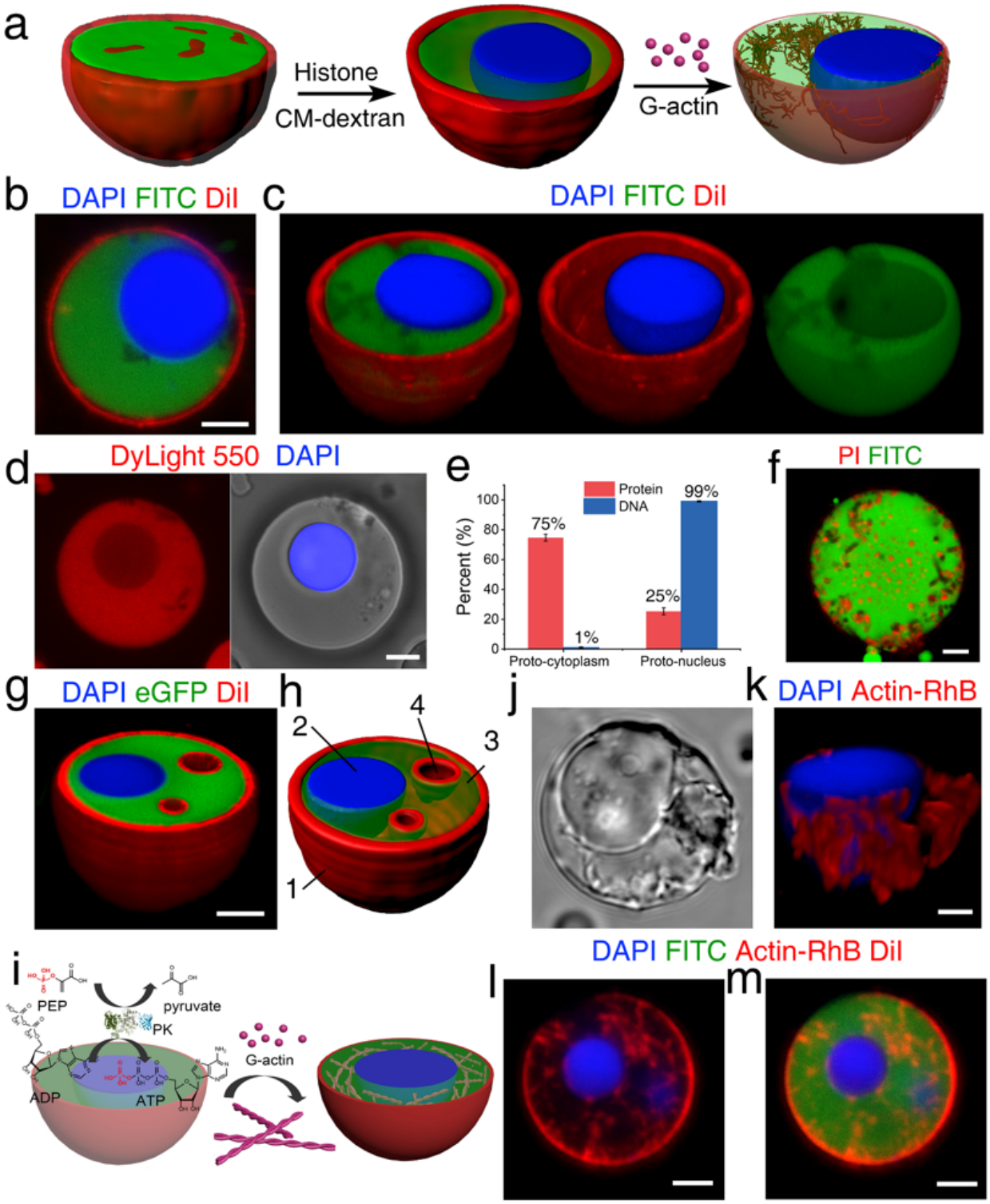

Figure 4

On-site augmentation of bacteriogenic protocells. a, Bacteriogenic protocells (left, outer membrane (red), proto-cytoplasm (green)) are structurally remodelled by endogenous DNA/histone liquid-liquid phase separation (centre) and energy-driven supramolecular assembly of GTP monomers (right) to produce a bacterial DNA/histone “proto-nucleus” (blue) and 3D network of proto-cytoskeletal filaments (brown). b, 2D confocal fluorescence microscopy image of a single histone/DNAase/MnCl2-containing bacteriogenic

protocell recorded 20 min after addition of FITC-CM-dextran. A single nucleus-like bacterial DNA/histone condensate (blue fluorescence, DAPI stain) is observed within the CM-dextran-enriched cytoplasmic-like (green fluorescence). Red fluorescence (DiI stain) corresponds to PA01-derived lipids on the outer membrane. c. Red/green- (left), red/blue- (right) and green- (left) filtered 3D images of the single bacteriogenic protocell displayed in b showing spatial segregated cytomimetic structures. d, Confocal fluorescence microscopy images showing partial exclusion of bacterial proteins (DyLight 550 stain, red fluorescence) from the DNA/histone condensate (blue). e, Histogram showing percentage of bacterial protein and DNA contents in the cytoplasmic-like and proto-nucleus like regions of bacteriogenic protocells. Number of samples, n= 3; error bars, standard deviations. f, Confocal fluorescence microscopy image of a single bacteriogenic protocell prepared as in b but in the absence of DNAase I and $MnCl_2$. Multiple DNA/histone condensates (red fluorescence, PI stained) are distributed throughout the CM-dextran-enriched proto-cytoplasm (green fluorescence). g,h 3D confocal fluorescence microscopy (g) and 3D Imaris reconstruction (h) images of a single bacteriogenic protocell under hypotonic conditions. Labels: 1, proto-cytomembrane; 2, proto-nucleus; 3, proto-cytoplasm (including CM-dextran); 4, water-filled vacuole. Staining as in (b) except green fluorescence originates from bacterially expressed eGFP. i, Schematic of F-actin assembly in PDDA/UTP-based bacteriogenic protocells containing an enzyme-mediated ATP-generation pathway. The protocells are prepared in the absence of ATP but charged with PK, PEP and ADP. PK-mediated transfer of phosphate from PEP to ADP yields pyruvate and ATP. Uptake of G-actin and Mg^{2+} results in ATP-associated polymerization and micro-filament assembly throughout the proto-cytoplasm but not within the DNA/histone proto-nucleus. j,k, Bright field confocal microscopy image (j) and corresponding 3D confocal fluorescence microscopy (k) images showing a single bacteriogenic protocell prepared as in (i). F-actin network (red fluorescence, RhB-labelled filaments), DNA/histone proto-nucleus (blue fluorescence, DAPI stain). l,m 2D confocal fluorescence microscopy images of a single bacteriogenic showing proto-cytoskeletal network (red fluorescence, RhB-labelled actin), membrane-free DNA/histone condensate (blue fluorescence, DAPI stain), PA01-derived outer membrane (red fluorescence, DiI stain) and proto-cytoplasm (green fluorescence, FITC-CM-dextran). All scale bars, 5 μm.

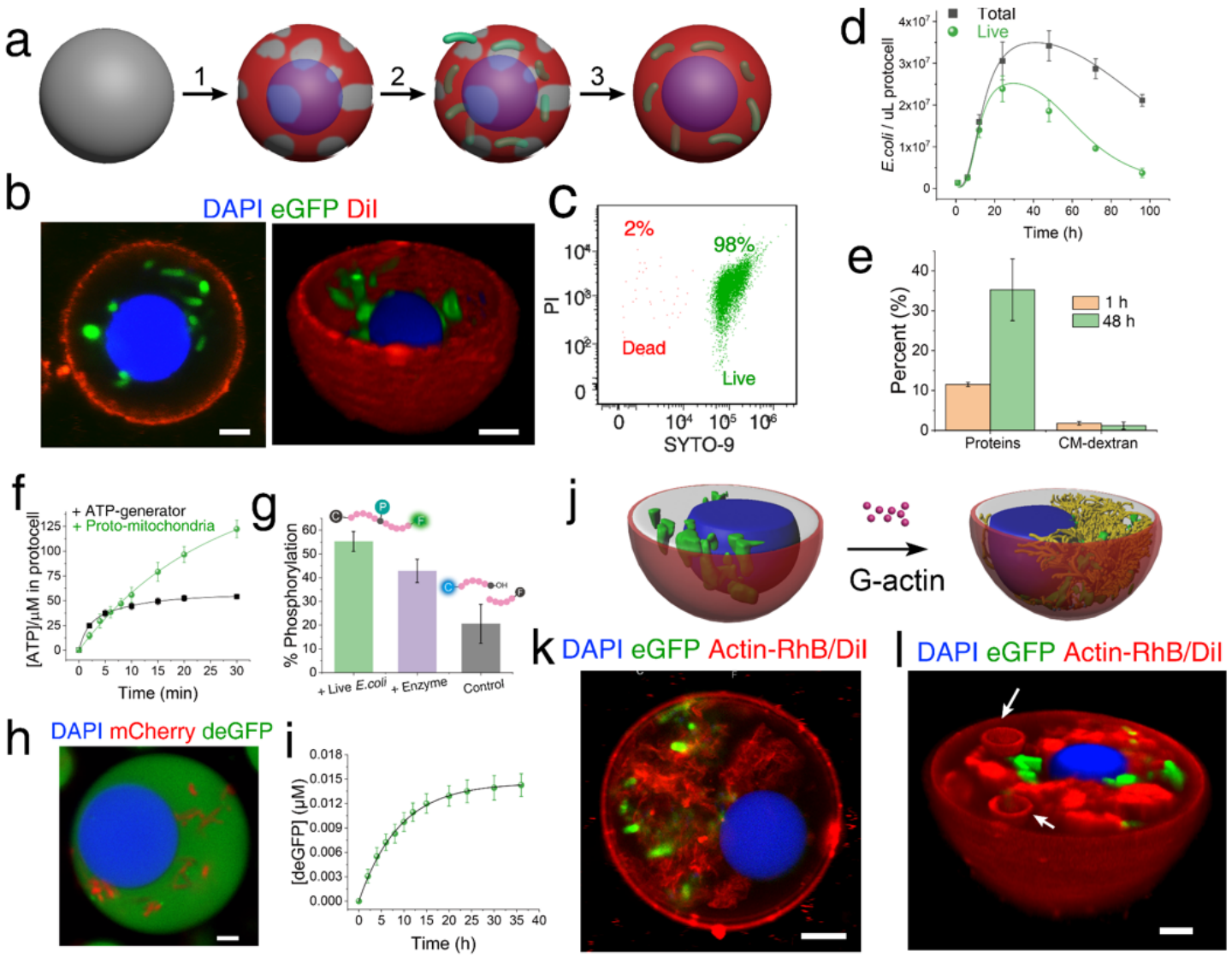

Figure 5

Live cell energization of bacteriogenic protocells. a, Implantation of living E. coli cells in bacteriogenic protocells. 1; construction of bacteriogenic protocells with DNA/histone sub-compartment and incomplete PA01-derived membrane. 2, penetration of living E. coli and capture within the proto-cytoplasmic region of the protocells. 3, addition of PA01-derived lipids and sealing of the protocell membrane. The bacteriogenic protocells were prepared from PDDA/UTP coacervate droplets and treated with lysozyme and melittin inhibitors to minimize lysis activity after subsequent addition of the live E. coli cells. b, 2D (left) and 3D (right) confocal fluorescence images showing the presence of E. coli-eGFP cells (green fluorescence) in the proto-cytoplasmic regions of a single bacteriogenic protocell after resealing of the outer membrane (red fluorescence, DiIC18 staining). The E. coli cells are excluded from the DNA/histone proto-nucleus (blue fluorescence, DAPI stained DNA). c, FACS live/dead fluorescence-gated analysis of bacteriogenic protocells containing SYTO/PI-stained E. coli cells. Most of the implanted bacteria (98%) remain alive after 3 h. d, Time-dependent plots of mean numbers of E. coli cells (total, grey; live, green). Number of samples, n = 3; error bars are standard deviations. e, Weight percentage of

proteins (BCA Protein Assay) and CM-dextran (FITC-labelled, fluorescence intensity) in bacteriogenic protocells after incubation for 1 h (orange) and 48 h (green), respectively. Number of samples, n = 3; error bars are standard deviations. f, Time-dependent plots of ATP concentration produced in PDDA/UTP-based bacteriogenic protocells via endogenous bio-generation (entrapped live E. coli cells (surrogate mitochondria), green dots) or chemical (enzyme) processing (PK/PEP/ADP pathway, black squares). Number of samples, n = 3; error bars are standard deviations. g, Kinase activity in PDDA/UTP bacteriogenic protocells; plots show percentage Ser/Thr pentapeptide phosphorylation associated with endogenous ATP bio-generation (entrapped live E. coli cells (+), green column, 55%), endogenous ATP chemical (enzyme) generation (PK/PEP/ADP pathway, purple column, 43%) or ATP present in the released bacterial lysate (no live E. coli, grey column, 21%). Number of samples, n = 3; error bars are standard deviations. h, Confocal fluorescence microscopy image of a single hybrid protocell with DNA/histone sub-compartment (blue fluorescence, DAPI staining) and entrapped living E.coli cells (strain DH2, red fluorescence (expressed mcherry)) displaying in vitro gene expression of deGFP (green fluorescence) in the proto-cytoplasmic region. i, Plot showing time-dependent increase in deGFP concentration over 40 h for a population of hybrid protocells. Data are fitted to an exponential decay curve; [deGFP]max = 0.015 μM, t1/2 = 9 h. Number of experiments, n= 3; error bars, standard deviations. j, Schematic of F-actin assembly in PDDA/UTP-based bacteriogenic protocells containing ATP-generating live E. coli cells (green) and a DNA/histone proto-nucleus (blue). k, 2D Confocal fluorescence microscopy image of a single living/synthetic cell construct with F-actin micro-filament network (red fluorescence, RhB-labelled actin) throughout the cytoplasmic-like space. The DNA/histone sub-compartment (blue fluorescence) and guest eGFP-E.coli cells (green fluorescence, expressed GFP) are immobilized within the cytoskeletal-like matrix. l, 3D confocal fluorescence microscopy image of a single bacteriogenic hybrid protocell exposed to hypotonic conditions for 30 min showing presence of pre-formed lipid membrane-coated water vacuoles (white arrows) trapped within the remodelled proto-cytoplasmic space. All scale bars, 5 μm

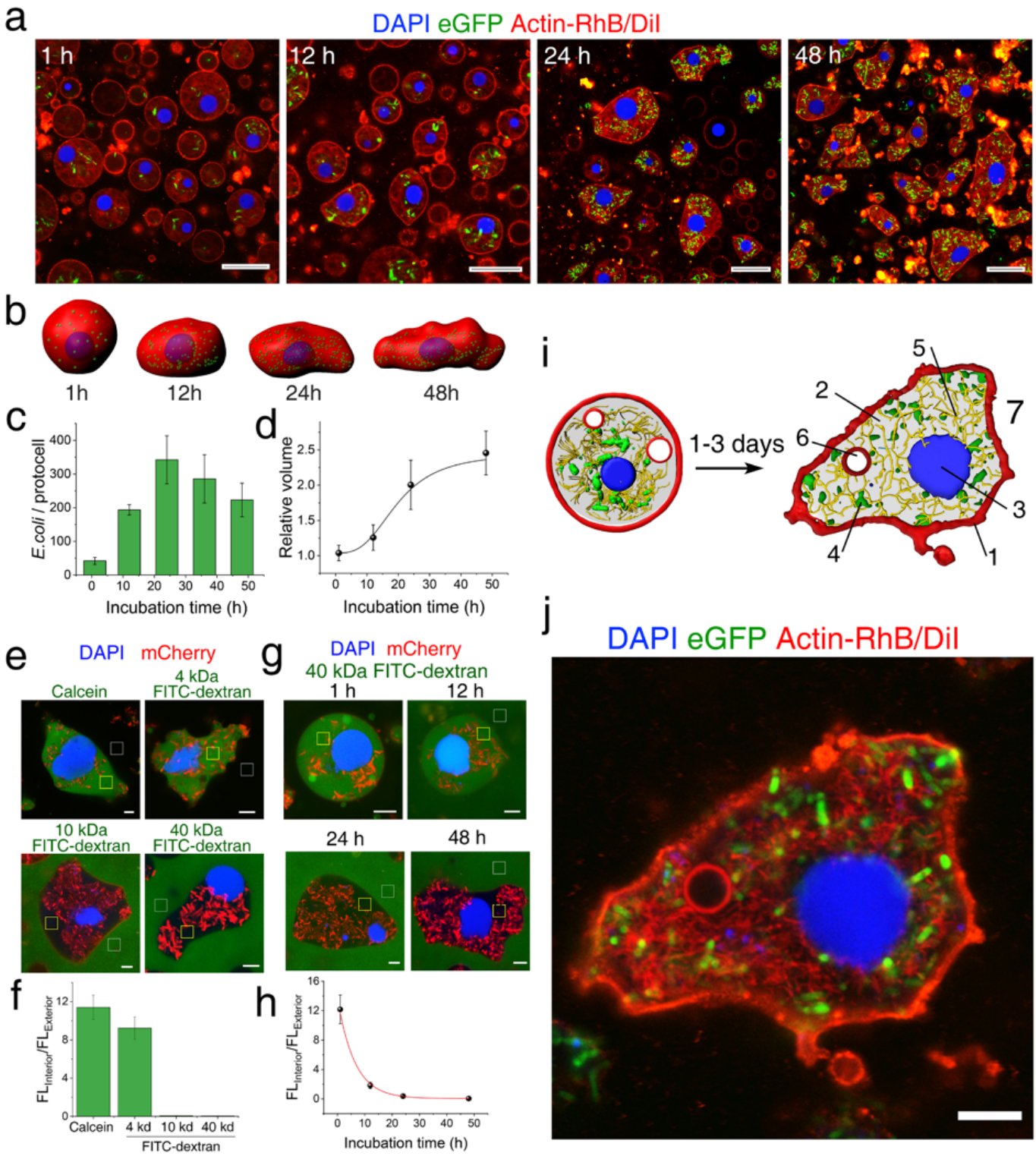

Figure 6

Live cell-mediated morphogenesis in bacteriogenic protocells. a, Time-series of confocal fluorescence microscopy images of spherical bacteriogenic protocells with entrapped E. coli-eGFP cells and F-actin (1 h) showing progressive transformation (12-48 h) into amoeba-like living/synthetic microscale construct due to on-site E. coli activity. Data recorded at given time intervals from different populations. Staining: F-actin (RhB, red fluorescence); DNA/histone condensate (DAPI, blue fluorescence); guest live E.coli cells

(eGFP, green fluorescence); outer membrane (DiIC18, red fluorescence). b, Corresponding time-series of 3D reconstruction images; colours as for stains shown in (a). c, Histogram of time-dependent changes in numbers of live E. coli cells per protocell; n = 3; error bars are standard deviations. d, Time-dependent plot of relative volumes for single living/synthetic constructs. Number of samples, n = 3; error bars are standard deviations. e,f, Confocal fluorescence microscopy images of single living/synthetic constructs incubated for 48 h followed by addition of various green-fluorescent solutes to the external phase (e), and corresponding uptake ratios (grey-value ratios, (FLinterior/FLexterior) (f), showing impermeability of 10 and 40 kDa FITC-dextran. g, as for (e) but after different periods of biological activity followed by addition of 40 kDa dextran. h, Corresponding uptake ratios determined for different incubation times shown in (g); uptake is inhibited after 20 hr of pre-treatment. i, j, Graphic (i) and corresponding 2D confocal fluorescence microscopy image (j) showing functional protoliving synthetic cell with seven cytomimetic features: 1, outer membrane; 2, molecularly crowded proto-cytoplasm; 3, proto-cytoskeleton; 4, membrane-free DNA/histone proto-nucleus; 5, surrogate mitochondria (E. coli cells); 6, membrane-bounded spherical water vacuoles; 7, amoeba-like cell morphology. All scale bars, 10 μm.

Supplementary Files

This is a list of supplementary files associated with this preprint. Click to download.

- MANNMethods.docx
- SupplementarydataFullproteinlistsinbacteriaandprotocells.xlsx
- Videos.zip
- MANNSupplementaryFigures.docx